PCCP

Accepted Manuscript

This is an *Accepted Manuscript*, which has been through the Royal Society of Chemistry peer review process and has been accepted for publication.

Accepted Manuscripts are published online shortly after acceptance, before technical editing, formatting and proof reading. Using this free service, authors can make their results available to the community, in citable form, before we publish the edited article. We will replace this *Accepted Manuscript* with the edited and formatted *Advance Article* as soon as it is available.

You can find more information about *Accepted Manuscripts* in the Information for Authors.

Please note that technical editing may introduce minor changes to the text and/or graphics, which may alter content. The journal's standard Terms & Conditions and the Ethical guidelines still apply. In no event shall the Royal Society of Chemistry be held responsible for any errors or omissions in this *Accepted Manuscript* or any consequences arising from the use of any information it contains.

ROYAL SOCIETY OF CHEMISTRY

www.rsc.org/pccp

Rational design of D−A$_1$−D−A$_2$ conjugated polymers with superior spectral coverage
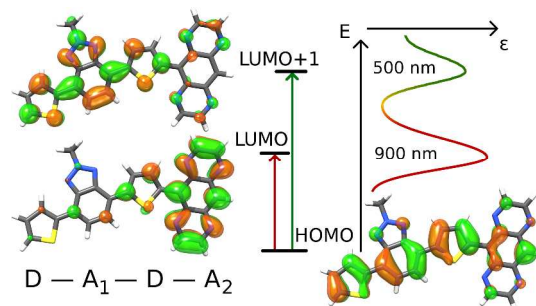
Svante Hedström,[a] Qiang Tao,[b] Ergang Wang,[b] and Petter Persson[a]*

[a]Division of Theoretical Chemistry, Lund University. P. O. Box 124, S-221 00 Lund, Sweden.

[b]Department of Chemistry and Chemical Engineering/Polymer Technology, Chalmers University of Technology, S-412 96 Göteborg, Sweden

*E-mail: petter.persson@teokem.lu.se Telephone: +46-462223311.

Table of contents entry

Calculations and experiments elucidate factors governing how D−A$_1$−D−A$_2$ polymers offer fundamentally improved spectral coverage via allowed transitions to both acceptor LUMOs.

Abstract

The spectral coverage of a light-harvesting polymer largely determines the maximum achievable photocurrent in organic photovoltaics, and therefore constitutes a crucial parameter for improving their performance. The $D–A_1–D–A_2$ copolymer motif is a new and promising design strategy for extending the absorption range by incorporating two acceptor units with complementary photoresponses. The fundamental factors that promote an extended absorption are here determined for three prototype $D–A_1–D–A_2$ systems through a combination of experimental and computational methods. Systematic quantum chemical calculations are then used to reveal the intrinsic optical properties of ten further $D–A_1–D–A_2$ polymer candidates. These investigated polymers are all predicted to exhibit intense primary absorption peaks at 615–954 nm, corresponding to charge-transfer (CT) transitions to the stronger acceptor, as well as secondary absorption features at 444–647 nm that originate from CT transitions to the weaker acceptors. Realization of $D–A_1–D–A_2$ polymers with superior spectral coverage is thereby found to depend critically on the spatial and energetic separation between the two distinct acceptor LUMOs. Two promising $D–A_1–D–A_2$ copolymer candidates were finally selected for further theoretical and experimental study, and demonstrate superior light-harvesting properties in terms of significantly extended spectral coverage. This demonstrates great potential for enhanced light-harvesting in $D–A_1–D–A_2$ polymers *via* multiple absorption features compared to traditional D–A polymers.

Introduction

Organic photovoltaics (OPV) offer a clean, renewable source of energy, with a reduced associated cost and complexity of manufacturing compared to silicon p–n junction solar cells.

The cell parameter most strongly associated with high efficiency is the short circuit current,[1] which in turn is largely determined by the spectral coverage of the polymer. The donor–acceptor (D–A) motif is the currently dominant polymer category for OPV applications,[2–5] with reported power conversion efficiencies (PCE) up to 10%.[6] The success of D–A polymers for device applications is largely due to their band gaps typically being narrower compared to homopolymers such as polythiophenes, allowing them to absorb a greater part of the solar emission and produce greater photocurrents. The small band gaps are achieved by incorporating one electron-rich (donor) and one electron-poor aryl unit (acceptor) along the backbone, where the donor and acceptor are respectively responsible for elevated highest occupied molecular orbital (HOMO) and deep lowest unoccupied molecular orbital (LUMO) energies of the copolymer. Electron transitions from HOMO to LUMO, with associated charge-transfer (CT) to the acceptor unit, are responsible for the strong low-energy absorption peak typically present in D–A polymers. Secondary absorption peaks of non-CT, $\pi \rightarrow \pi^*$ character tend to be of wavelengths ≤ 400 nm, giving negligible contribution to the photocurrent due to poor overlap with the solar emission spectrum.

D–A polymers constitute an improvement in spectral coverage compared to homopolymers, but further enhancement of OPV photocurrents is still feasible by means of broader effective absorption. This has in part been accomplished by fabrication of tandem solar cells,[7–10] where two subcells using different polymers with complementary absorption profiles together exploit a larger part of the solar emission. These are however considerably more complicated and expensive to manufacture than single junction OPVs. Another strategy for broadening the light-response of OPVs is to blend two D–A polymers into the same bulk heterojunction active layer, fabricating either pure polymer–polymer cells,[11–13] or ternary systems with a fullerene

acceptor.[14,15,16] The efficiency of these two types of OPVs is still limited, due to added complexity in controlling *e.g.* morphology and carrier transport.[17,18–20]

Extending the spectral coverage while circumventing the issues with fabrication and morphology associated with tandem, ternary, and polymer–polymer cells, is possible using copolymers with more than one acceptor unit along the backbone, either as random copolymers,[21–24] or less commonly as strictly alternating D–A_1–D–A_2 polymers.[25–32] These are highly promising for OPV applications, we recently reported a 7.0 % PCE for the P3TQTI-F polymer,[33] the most efficient D–A_1–D–A_2 polymer to date. This motif is fundamentally advantageous for the potential of two absorption peaks in the spectral region of strong solar emission.[33,34]

The presence of two peaks in D–A_1–D–A_2 polymers originate from strongly allowed electronic CT transitions to two distinct unoccupied MOs, yielding superior spectral coverage at relevant wavelengths ≥ 450 nm, see Figure 1. We recently showed that LUMO and LUMO+1 of D–A_1–D–A_2 polymers agree in shape and energy to the respective LUMOs of corresponding D–A polymers.[33] According to a molecular orbital (MO) argument, the two acceptor LUMOs will interact and mix, forming two polymer LUMOs with larger energy separation. The mixing coefficient λ is proportional to the spatial overlap and the inverse of the energy separation $\Delta E_{LUMO,A}$ of the non-interacting acceptor LUMOs, as outlined in Equation 1.[35]

$$\lambda_{LUMO-LUMO} \cong \frac{k\langle \varphi_{LUMO,A_1}|\varphi_{LUMO,A_2}\rangle}{E_{LUMO,A_2} - E_{LUMO,A_1}} \propto \frac{e^{-\beta R(A_1-A_2)}}{\Delta E_{LUMO,A}} \tag{1}$$
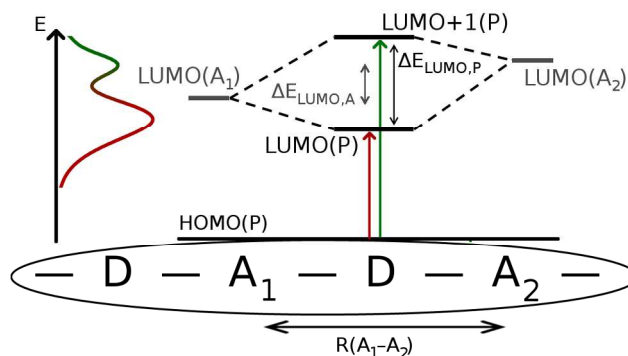
Figure 1. Schematic description of the energy levels involved in D–A$_1$–D–A$_2$ polymers. While the HOMO is typically delocalized across the backbone, the two acceptor LUMOs interact, forming the copolymer LUMO and LUMO+1 with slightly altered energies but largely retained character. Improved spectral coverage is obtained if electronic transitions to both polymer LUMO (red) and LUMO+1 (green) are allowed.

The development of new D–A$_1$–D–A$_2$ designs with improved light-harvesting properties requires better insight into the special optical features of D–A$_1$–D–A$_2$ polymers, in combination with screening of more new candidate systems, typically relying on time-consuming synthetic and experimental characterization work. Light-harvesting traits of polymers such as the intensity and energy of excitations, the resulting spectra, as well as structural and electronic properties, *e.g.* molecular orbitals can however all be accurately and efficiently calculated using density functional theory (DFT).[36–40] While calculations have traditionally served as an explanatory tool for experimental findings, they can also be exploited to guide the pursuit of polymer candidates with superior spectral properties.[36]

In this article, we use DFT calculations to explore the fundamental properties of the new class of D–A$_1$–D–A$_2$ copolymers, providing guidelines to the ongoing development of new and efficient

light-harvesting polymers. The electronic and optical properties of 15 such copolymers are scrutinized based on extrapolations of oligomer calculations to the polymer limit. First, we examine three previously reported D–A_1–D–A_2 polymers and their qualitatively different spectral responses, where good agreement between calculations and reported experimental data serves as validation of the computational methodology. Second, we present and study 10 new D–A_1–D–A_2 polymer designs, focusing on the structure–property relation with respect to substantial absorptivity over a wide spectral region, and a molecular scale insight into the relevant orbitals that govern the electronic transitions. Finally, two promising D–A_1–D–A_2 polymers are subjected to extended experimental and computational investigation, confirming our strategy to broaden the spectral response by two allowed low-energy excitations, having profound implications for the photocurrents and efficiencies of OPVs.

Methods

Computational details

All calculations were made with the Gaussian 09 program package.[41] Monomer and dimer model systems of D–A_1–D–A_2 polymers were fully optimized at the DFT[42] PBE0[43]/6-31g(d,p)[44] level of theory. They were subsequently subjected to a scheme of time-dependent (TD)-DFT[45] in its linear-response formalism,[46–48] calculating the transition wavelengths λ and oscillator strengths f of the oligomers. D–A polymers underwent the same treatment, for oligomers of 1–2 repeating units for PTI-1, 1–3 repeating units for P3TPhQ and PTPzQ, and 1, 3, and 4 repeating units for PTBTz and PTBT. The three D–A_1–D–A_2 polymers in the second results-subsection dedicated to validation of the theoretical protocol: PTQTI, PBTDPP, and PBBTDPP, additionally underwent

corresponding optimizations+TD-DFT at the ωB97XD/6-31G(d,p) level of theory, as well as at the PBE0/6-31G(d,p)+PCM(CHCl$_3$) level. All five polymers that at some point were compared to experiments: PTQTI, PBTDPP, PBBTDPP, P3TQTIF, and PTIIBTzF also underwent frequency calculations post optimizations to warrant that a structural optimum was reached.

Calculated UV/vis absorption spectra were simulated for all oligomers by applying to each calculated transition an inhomogeneous Gaussian shape broadening with a total width of 4000 cm^{-1}, where the inhomogeneity is obtained by applying a 4800 cm^{-1} FWHM broadening to the blue side of each transition and 3200 cm^{-1} towards the red. This is done in order to mimic the experimental inhomogeneous distribution of conformations and unresolved vibronic progression that together confer a slower decay towards bluer wavelengths in experimental absorption peaks. Furthermore, the relation between the dimensionless f and mass extinction coefficients (ε) was exploited, as outlined in Equation 2,[49] where m$_e$ and q$_e$ are the electron mass and charge, ε$_0$ is the vacuum permittivity, N$_A$ is the Avogadro number, ν is the photon frequency, and M is the molecular mass.

$$f = \frac{4\ln(10)m_e c\varepsilon_0 M}{N_A q_e^2} \times \int \varepsilon(\nu)d\nu \qquad (2)$$

The calculated oligomer first peak E$_{abs}$=hc/ λ and ε$_{max}$ were plotted *vs.* the inverse number of repeating units (1/n), and the best linear fits were extrapolated to 1/n→0, *i.e.* infinite polymer length, as described in the literature.[36,50–52]

Although the PBE0 functional has been used successfully for studies of conjugated polymers,[36,53,54,55] being a standard hybrid DFT functional it tends to overestimate the conjugation and planarity, and consequently also the absorption λ and ε. We have recently introduced an empirical correction that compensates for this systematic overestimation, combined

with the overestimation resulting from using fully optimized structures corresponding to a 0 K temperature.[36] The correction is based on the extrapolated first peak E_{abs} and ε_{max} which are respectively blue-shifted by +0.32 eV and downscaled by a factor of 1.6, as per Equation 3.

$$\varepsilon_{corr}\left(E_{abs,corr}\right) = \frac{\varepsilon_{extrapol}\left(E_{abs,extrapol} + 0.32\ eV\right)}{1.6} \tag{3}$$

The oligomer size (1 or 2 repeating units for $D–A_1–D–A_2$ polymers, 2, 3, or 4 for D–A polymers) whose uncorrected, PBE0-calculated first peak E_{abs} best agrees with the extrapolated and corrected $E_{abs,corr}$, had its spectrum parallel-shifted to that its first peak matches $E_{abs,corr}$, and scaled to match $\varepsilon_{max,corr}$. For the $D–A_1–D–A_2$ polymers whose extrapolated E_{abs} falls between the calculated mono- and dimer spectra, the procedure was done for both sizes, and the average of the two spectra was used.

The $PC_{71}BM$ absorption spectrum was calculated at the TD-PBE0/6-31g(d,p)//PBE0/6-31g(d,p) level, applying a homogenous Gaussian broadening of 3000 cm^{-1}.


Material characterization

^{1}H NMR (400 MHz) and ^{13}C NMR (100 MHz) spectra were acquired using a Varian Inova 400 MHz NMR spectrometer. Tetramethylsilane was used as an internal reference with deuterated chloroform as the solvent. Size exclusion chromatography (SEC) was performed on an Agilent PL-GPC 220 Integrated High Temperature GPC/SEC System with refractive index and viscometer detectors. The columns are 3 PLgel 10 μm MIXED-B LS 300×7.5 mm columns. The eluent was 1,2,4-trichlorobenzene. The working temperature was 150 °C. The molecular weights

were calculated according to relative calibration with polystyrene standards. UV-Vis absorption spectra were measured with a Perkin Elmer Lambda 900 UV-Vis-NIR absorption spectrometer.

Results

Acceptor unit strength

The copolymer LUMO energy is crucial for solar cell performance, since its offset *vs.* the fullerene LUMO energy provides a driving force for charge transfer at the polymer–fullerene interface, and also because it partly determines the optical band gap of the copolymer. The copolymer LUMO is mainly determined by the acceptor unit, whose LUMO energy thus roughly indicates the strength of the acceptor. $D–A_1–D–A_2$ polymers rely on their two acceptors having different strength, so that their spectral responses complement each other. In total, we use eight different two-acceptor combinations of seven different acceptor units. These are benzo[1,2-c;4,5-c′]bis[1,2,5]thiadiazole (BBT), 2,1,3-benzothiadiazole (BT), 2-alkyl-benzo[d][1,2,3]triazole (BTz), 2,5-dialkyl-1,4-diketopyrrolo[3,4-c]pyrrole (DPP), N,N′-dialkyl-isoindigo (II), 2,3-bis-(3-alkoxyphenyl)quinoxaline (PhQ), pyrazino[2,3-g]quinoxaline (PzQ). Their molecular structures are shown in Chart 1, together with thiophene (T) which acts as donor in all polymers, either as a single unit, as bithiophene (2T), or as terthiophene (3T). Probing donors with varying lengths is important, since these act not only as electron donors, but also spatial separators between the acceptors.

Chart 1. Structures of the studied donor unit (T) and the 7 acceptor units.
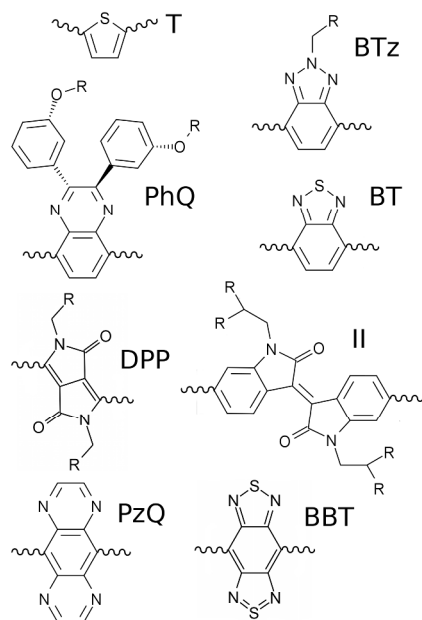
The calculated HOMO and LUMO energies of the isolated acceptor units used in this study are presented in Table 1 together with peak wavelengths λ_{max} in solution for typical D–A polymers incorporating the respective acceptors. Calculated $E_{LUMO,A}$ are in good trend-wise agreement with the calculated λ_{max}, while no such correlation appears between λ_{max} and the acceptor unit HOMO–LUMO gap. This is rationalized from the fact that the copolymer HOMO energy is mainly determined by the donor unit. DPP induces longer λ_{max} in copolymers than indicated by its LUMO energy. This is partly due to the absence of steric hindrance from hydrogen atoms when DPP is coupled to thiophene-like donors, leading to more planar copolymer backbones, and partly because of the high HOMO energy of DPP. The LUMO of BTz is stabilized when substituted with electron withdrawing fluorine atoms, often decreasing the copolymer band gap. This band gap reduction is not apparent in all cases, since fluorination typically also lowers the copolymer HOMO energy.[25,56–58]

Table 1. The HOMO and LUMO energies of the acceptors as single molecules, calculated with

PBE0/6-31G(d,p). Peak absorption wavelengths λ_{max} and corresponding absorption energies

E_{abs}=hc/ λ_{max} in solution for typical D–A polymers incorporating the respective acceptor units.

Sorted by increasing LUMO energy, approximately corresponding to decreasing acceptor

strength.

Acceptor	HOMO [eV]	LUMO [eV]	H–L gap [eV]	E_{abs} range [eV]	λ_{max} range [nm]
BBT	-6.48	-3.44	3.04	1.45–0.95	850–1320[52,59,60]
PzQ	-6.80	-2.74	4.06	1.90–1.45	650–870[36,60,61]
II	-5.79	-2.59	3.20	2.25–1.70	550–720[62–64]
BT	-6.91	-2.21	4.70	2.60–1.75	480–700[65–67]
DPP	-5.70	-2.02	3.68	2.20–1.50	570–830[68,69]
PhQ	-6.08	-1.77	4.31	2.55–2.00	490–620[70–72]
BTzF	-6.76	-1.35	5.41	2.35–2.05	530–610[56,73–75]
BTz	-6.39	-1.04	5.35	3.10–2.15	400–580[56,76,77]

Origin of dual peak absorption in D–A$_1$–D–A$_2$ copolymers

Of the few reported strictly alternating D–A$_1$–D–A$_2$ polymers, some exhibit two absorption peaks

$\gtrsim$ 450 nm,[30,31,32] whereas others show photoresponses similar to D–A polymers, with only one

resolved low energy peak.[26–28,30,29,78] However, no detailed information regarding these spectral

features, rationalized from the nature of the electronic transitions, has been reported. To gain

insight into the molecular level structure–property relation with respect to dual absorption potential, three D–A_1–D–A_2 polymers from the literature were chosen for computational scrutiny: PBBTDPP[30] with two distinct low-energy peaks, as well as PTQTI[26,25] and PBTDPP,[30] each with only one resolved experimental peak. DFT and TD-DFT was used to explore how the electronic structure and optical properties of conjugated polymers are affected by including two acceptor units with distinct electronic traits.Computationally predicting polymer properties is difficult due to several differences in conditions. While experiments treat long and polydisperse chains in a solvent at finite temperatures, standard quantum chemical calculations are in contrast performed at 0 K, either in vacuum or with an implicit continuum solvent, and due to limitations in computational power, shorter oligomers are studied rather than the full polymer chains. Consequently, any strategy aiming to obtain computational results directly comparable to experimental data will by necessity introduce additional approximations, bringing associated uncertainties to the results. One such approximation, commonly used throughout the literature and also herein,[36,79–81] is the fitting of oligomer absorption energies some linear or non-linear (e.g. Hückel or Kuhn) type function of the reciprocal number of repeating units n, followed by extrapolation to $1/n=0$, i.e. the polymer size limit.

Due to the above mentioned differences in conditions between experiments and calculations with respect to e.g. finite temperature and explicit solvent effects, calculations on fully optimized oligomers have been shown to yield a systematic underestimation of absorption energies and overestimation of absorption strengths,[36,55] which also partly is due by shortcomings in standard hybrid DFT functionals. An empirical correction scheme, outlined in Equation 3,[36] has previously been developed to compensate for these systematic overestimations of wavelengths λ and absorption coefficients ε, and we here apply this correction to obtain better quantitative spectral

predictions. The empirical correction is developed for application to gas phase PBE0 calculations, but we also probe the effect of an implicit solvent in form of a polarizable continuum medium (PCM). As shown with lists of transitions in the ESI, the addition of the solvent to the calculations confers a consistent but small red-shift of the transitions and thus absorption peaks, and strengthens the transitions somewhat.

The contribution to the λ and ε overestimations stemming from the hybrid PBE0 functional is related to the self-interaction error in DFT.[82–85] This can be partly overcome by using long-range corrected (LC) functionals, which are suggested to give a better description of transitions involving some CT.[86–88] However, most out-of-the-box LC functionals come with a LC parameter of ω=0.3–0.5, which is suitable for small molecules but too large for extended systems such as conjugated polymers.[87,89] We have here tried one such LC functional, ωB97XD, and compared the results to those obtained with PBE0 including the empirical correction, *vide supra*.

Clearly, the ωB97XD results significantly overestimate the absorption energies, due to shortcomings of both structural (less planar geometries) and electronic origins (in the TD-DFT procedure), both effects attributed to a too large LC parameter as per above. This band gap overestimation is rather unphysical, since 0 K temperature calculations should promote smaller E_{abs} than observed in the room-temperature experiments.[55] Conversely, the results from PBE0 with the empirical correction show for all three polymers PTQTI, PBTDPP, and PBBTDPP an excellent agreement to experiments with respect to relative peak heights and peak wavelengths, as seen in Figure 2a and b, though this may in part be due to fortuitous cancellations of error related to the uncertainties outlined above. Although the agreement serves as a partial validation of the empirical correction scheme, independently of the test set with which it was developed, it is still uncertain whether it is universally applicable, a question for future studies. The

Physical Chemistry Chemical Physics Accepted Manuscript

experimental absorption coefficients for PBTDPP and PBBTDPP have not been reported, and for

PTQTI they are slightly lower compared to calculations. The qualitative (and to some extent

quantitative) agreement serves as a validation of our computational methodology, and encourages

its application in the continued investigation of the optical traits of the polymers in pursuit of

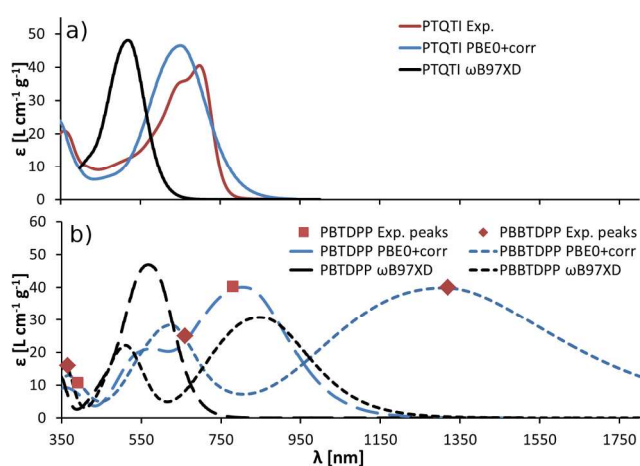insight into the potential for dual peak absorption and superior light-harvesting.

Figure 2. Calculated and experimental absorption spectrum for PTQTI (a). Calculated spectra of

PBTDPP and PBBTDPP, with experimental peak positions as taken from literature,[30] and

normalized to the same first peak ε_{max} as the calculations (b). Calculated spectra are obtained as

outlined in the Methods section, based on the empirical correction in Equation 3.

The first (lowest energy) calculated absorption peak positions for the three $D–A_1–D–A_2$ polymers

are mainly governed by the stronger acceptor, falling within the λ_{max} range of typical

corresponding D–A polymers, as listed in Table 1. Furthermore, the second peak at 624 nm for

PBBTDPP and the shoulder at ~570 nm for PBTDPP both coincide with the peak wavelengths

displayed by DPP-containing D–A polymers (see Table 1), indicating a direct link between the weaker acceptor in D–A_1–D–A_2 polymers and the second absorption feature. In the PTQTI spectrum however, only one discernable peak appears.

To elucidate the reasons for the qualitatively different spectral profiles of the three D–A_1–D–A_2 polymers, their calculated electronic transitions were examined on the mono- and dimer levels. Monomer excitation data is presented, see Table 2, since orbitals and transitions are of more pure character in smaller systems, being therefore easier to analyze, although oligomers of two repeating units often are more representative of experimental polymers, and in better quantitative agreement. All monomers exhibit an intense first transition of mainly HOMO→LUMO character, whereas the HOMO→LUMO+1 transition is very weak for PTQTI but strongly allowed for PBTDPP and PBBTDPP. Excitations $\gtrsim$ 450 nm are typically of non-CT, $\pi \rightarrow \pi^*$ character, and are not significant for solar cell performance since the solar emission lacks intensity at such short wavelengths.

Table 2. Wavelengths and oscillator strengthsof relevant calculated transitions for the three D–A_1–D–A_2 polymers, as calculated for the monomers.[a] Also the dominant orbital contributions and the percentage of that orbital contribution C, calculated as the square of the expansion coefficient. The first transition in PBBTDPP shows a > 100 % character of H→L excitation which is due to the presence of a corresponding L→H deexcitation for that transition.

PTQTI				PBTDPP				PBBTDPP			
λ_{abs} [nm]	f	Orbitals	C [%]	λ_{abs} [nm]	f	Orbitals	C [%]	λ_{abs} [nm]	f	Orbitals	C
582.4	1.03	H→L	93.5	660.0	1.10	H→L	97.6	1070	0.66	H→L	10

494.1	0.09	H→L+1	84.3	538.3	0.62	H→L+1	87.7	573.9	1.02	H→L+1	96
347.0	0.24	H-4→L+1	40.1	378.8	0.14	H-2→L	62.1	398.2	0.16	H→L+3	77
341.5	0.15	H→L+3	29.6	336.0	0.18	H-2→L+1	60.7	347.1	0.24	H-2→L+1	43

a H=HOMO, L=LUMO.

The HOMO, LUMO, and LUMO+1 orbitals of the three D–A$_1$–D–A$_2$ monomers are depicted in

Figure 3 and their energies are listed in Table S1 in the ESI. In all cases, the HOMO is

delocalized across the backbone, promoting the important hole-mobility through the polymer

phase. The LUMO on the other hand, is more localized on the stronger acceptor, analogous to the

typical behavior of D–A polymers,[36,90–92] and the LUMO+1 orbitals are denser on the weaker

acceptors. The dimers (not shown) display qualitatively identical orbital distributions over the

respective acceptors, although their orbital energies differ from the monomers. The partial

localization of LUMO and LUMO+1 on the respective acceptors is most pronounced for

PBBTDPP where the difference in acceptor strength $\Delta E_{LUMO,A}$=-1.42 eV is largest. PTQTI and

particularly PBTDPP have smaller $\Delta E_{LUMO,A}$ of -0.82, -0.19 eV respectively, which in accordance

with Equation 1 enhances the LUMO(A$_1$)–LUMO(A$_2$) interactions, and consequently results in

more mixed and delocalized LUMO and LUMO+1 orbitals. Thus, the two absorption peaks for

PBBTDPP correspond to CT transitions to the LUMOs of the two respective acceptors. The

PBTDPP absorption is analogous, though the similar strength of its two acceptors leads to the

second absorption feature being unresolved, appearing only as a shoulder in the spectrum in

Figure 2. Table 2 demonstrates that PTQTI has a HOMO→LUMO+1 transition of negligible

intensity, despite its $\Delta E_{LUMO,A}$ being larger than that of PBTDPP, resulting in a single absorption
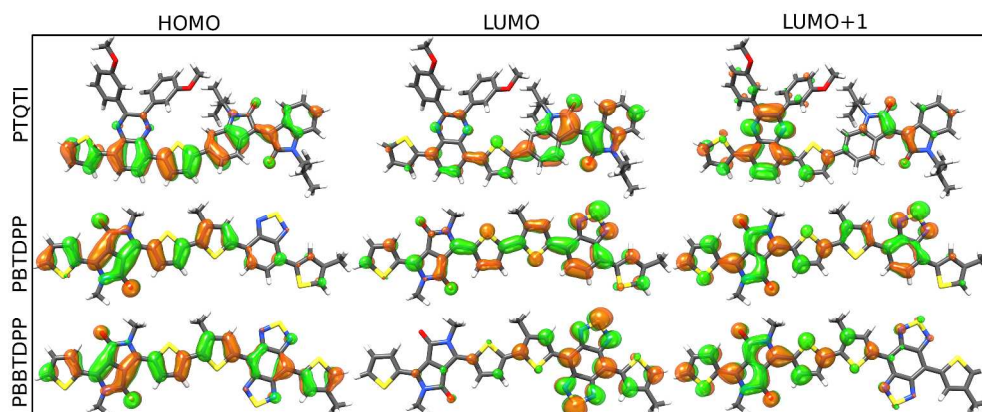
peak.

Figure 3. Frontier orbitals for the monomers of PTQTI, PBTDPP, and PBBTDPP.

Isovalue=0.025.

**Systematic screening of new D–A$_1$–D–A$_2$ copolymer designs**

In this section, systematic computational scrutiny of a larger set of D–A$_1$–D–A$_2$ polymers is used

to elucidate the factors that determine the potential for increased spectral coverage of this type of

polymers, and to provide computational guidance for promising D–A$_1$–D–A$_2$ structural designs.

To this end, an extended set of ten copolymers were selected, in five distinct two-acceptor

combinations with different resulting $\Delta E_{LUMO,A}$. The acceptors are separated by one or three

thiophene donor units, to permit probing of the effect of spatial acceptor separation R(A$_1$–A$_2$).

The weak BTz acceptor was used in eight of the ten polymers, expecting it to induce an

absorption contribution complementary to that of the stronger acceptors PhQ, BT, II, and PzQ.

The structures of the ten D–A$_1$–D–A$_2$ polymers are presented in Chart 2.

Chart 2. The structures of the 10 computational D–A$_1$–D–A$_2$ polymers. The donor (D) is either thiophene (T, n=1) or terthiophene (3T, n=3). R is an arbitrary alkyl side-chain.
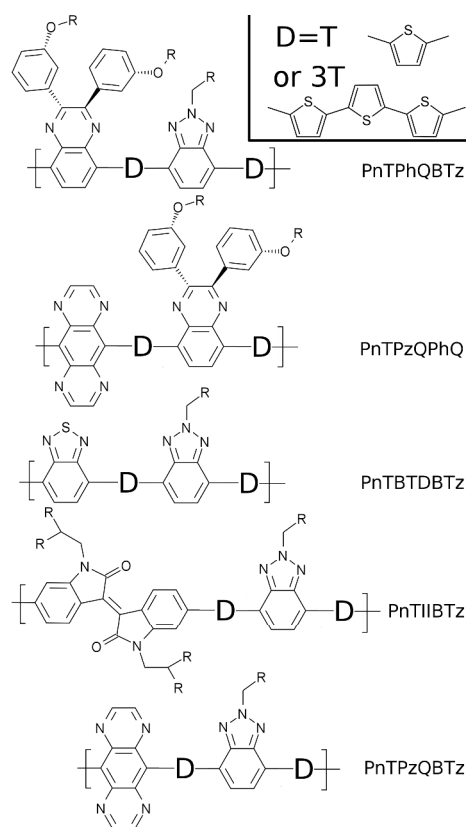
The absorption spectra of the polymers are presented in Figure 4, as obtained through extrapolations from mono- and dimer calculations, employing Equation 3. The polymers were modeled without long alkyl chains in the DFT calculations, but to estimate the mass extinction coefficients ε, an arbitrary side-chain mass was added, equal to a side-chain ratio of 33 wt% for all polymers. The spectra of the ten D–A$_1$–D–A$_2$ copolymers show large variations in shape, peak wavelength, maximum extinction coefficient, and resulting spectral coverage. In all cases, the polymers with one thiophene unit in the donor segments exhibit longer first peak λ_{max} than the corresponding polymer with 3T-donors. This trend is qualitatively understood from the distance

dependent LUMO(A$_1$)–LUMO(A$_2$) interactions described by Equation 1 and Figure 1, where a shorter donor induces a lower LUMO(polymer). This accounts also for the secondary peak/shoulders being considerably blueshifted, due to higher LUMO+1 conferred by a shorter donor segment.

The four polymers containing the very strong PzQ acceptor demonstrate very long λ_{max} of 866–954 nm, constituting a slight redshift compared to the typical absorption of D–PzQ polymers as listed in Table 1, which is attributed to that we omit phenyl side groups while they are normally included in synthesis of this acceptor. The first peak ε_{max} of the polymers with PzQ are however limited to around 40–50 Lg^{-1}cm^{-1}. Also PTBTBTz, PTPhQBTz, and P3TPhQBTz exhibit first peak λ_{max} (730, 681, and 643 nm respectively) longer than D–A polymers with those respective strongest acceptors: BT and PhQ. The 1st peak ε_{max} appears insensitive to the number of thiophenes, amounting to around 50, 65, 65, and 40 Lg^{-1}cm^{-1} for PnTPzQBTz, PnTIIBTz, PnTBTBTz, and PnTPzQPhQ, respectively. Only when PhQ is the stronger acceptor does the addition of two thiophenes noticeably increase 1st peak ε_{max}: from 32 to 49 Lg^{-1}cm^{-1}.
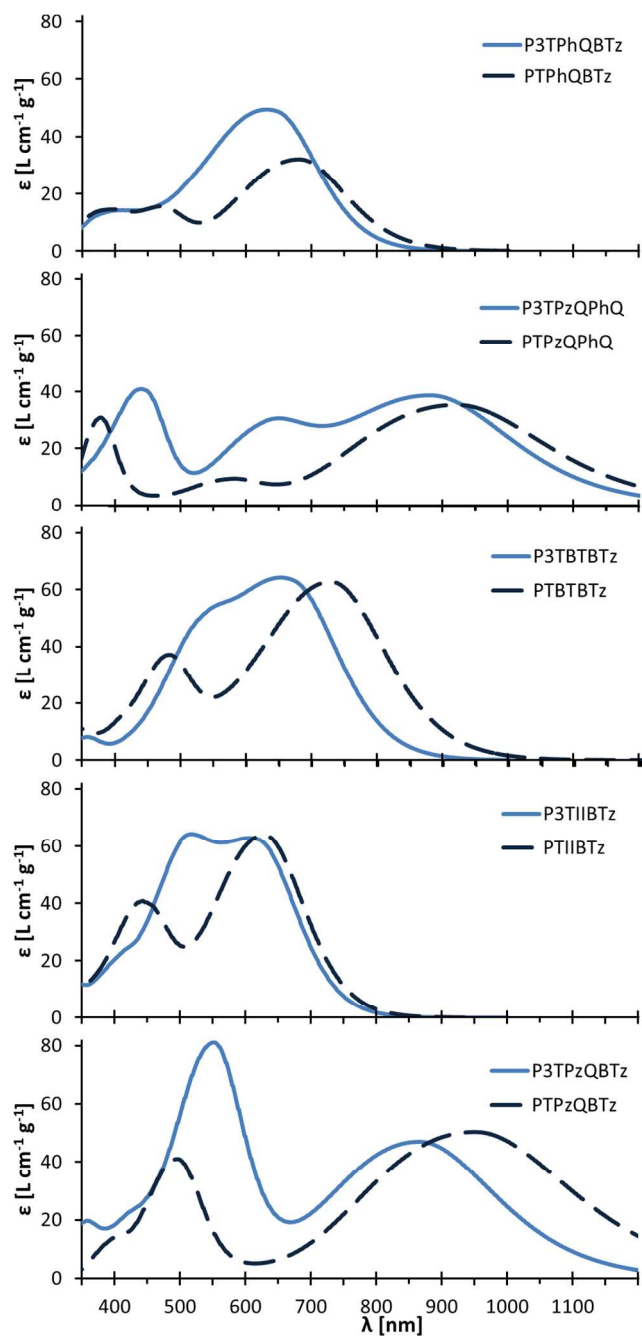
Figure 4. Absorption spectra of the 10 computationally studied D–A$_1$–D–A$_2$ polymers, as calculated with TD-DFT, employing Equation 3.

All polymer spectra in Figure 4 show some secondary spectral features $\gtrsim 450$ nm, though their intensities and wavelengths vary greatly, and for P3TBTBTz, and P3TPhQBTz they appear only as unresolved shoulders to the 1st peak. The secondary absorption peaks/shoulders exhibit a clear redshift when extending the donor segments, again relating to Equation 1. The origin of the secondary absorption features is elucidated in Table 3, where the first two transitions with non-negligible intensity for all monomers are listed. It is obvious that the first peaks for all polymers arise due to HOMO→LUMO transitions, whereas the second transitions are of dominantly HOMO→LUMO+1 character, validating the $D–A_1–D–A_2$ design strategy. Note that the 3T donor polymers at the monomer level give lower energy transitions compared to those with the shorter T donors, which is simply due to their longer repeating unit. For the extrapolated values the opposite is observed: the longer donor induces a slight blueshift, apparent in Figure 4.

Table 3. Monomer transitions responsible for the first two spectral features in polymers, with dominant orbital contributions and the percentage C of that contribution.[a]

PTPhQBTz				P3TPhQBTz			
λ [nm]	f	Orbitals	C [%]	λ [nm]	f	Orbitals	C [%]
491.6	0.63	H→L	97.1	578.1	1.78	H→L	94.1
408.8	0.39	H→L+1	95.9	503.5	0.60	H→L+1	96.5

PTPzQPhQ				P3TPzQPhQ			
623.5	0.43	H→L	98.5	813.6	0.97	H→L	96.6
483.1	0.16	H→L+1	97.0	592.8	0.45	H→L+1	70.5

PTBTBTz				**P3TBTBTz**			
507.2	0.66	H→L	98.0	626.4	1.51	H→L	93.2
408.6	0.54	H→L+1	96.4	512.6	1.09	H→L+1	87.5

PTIIBTz				**P3TIIBTz**			
572.3	0.96	H→L	92.5	640.5	1.72	H→L	88.9
426.4	0.77	H→L+1	89.0	510.1	1.12	H→L+1	86.6

PTPzQBTz				**P3TPzQBTz**			
644.3	0.48	H→L	99.0	800.2	0.90	H→L	96.4
413.1	0.33	H→L+1	41.4	523.6	1.52	H→L+1	95.2

[a]H=HOMO, L=LUMO.

As evident from Table 3, the two first, relatively intense excitations in all cases mostly correspond to transitions from HOMO to LUMO and LUMO+1 respectively. The delocalized HOMOs (see Figure S2 in the ESI) promotes good hole transport through the polymers. The HOMO, LUMO, and LUMO+1 energies are listed in Table S1 in the ESI. In agreement with our previous study,[33] each D–A$_1$–D–A$_2$ LUMO and LUMO+1 matches the corresponding D–A copolymer LUMO both in energy (Figure 5a) and in localization (Figure 5d). All polymers exhibit LUMOs mostly situated on the stronger acceptor (right hand side in Figure 5d), and LUMO+1s on the weaker acceptors. However, in analogy to Figure 3, the localization of these orbitals on the respective acceptors is only partial, appearing more localized for longer donors and larger $\Delta E_{LUMO,A}$ (further down in Figure 5d). This is consistent with the basic molecular

orbital argument outlined in Equation 1 and Figure 1, that the LUMOs of the two acceptor units

interact, forming the LUMO and LUMO+1 of the copolymers/oligomers. This LUMO(A_1)–

LUMO(A_2) mixing is more pronounced for small spatial and energetic separations of the

constituent orbitals. So for *e.g.* P3TPzQBTz, being the extreme case of large spatial and energetic

separation of the two acceptor LUMOs, the copolymer LUMO and LUMO+1 almost exclusively

resemble the respective PzQ and BTz LUMOs. In PTPhQBTz conversely, the copolymer LUMO

and LUMO+1 have significant character of both PhQ and BTz LUMO, due to the prominent

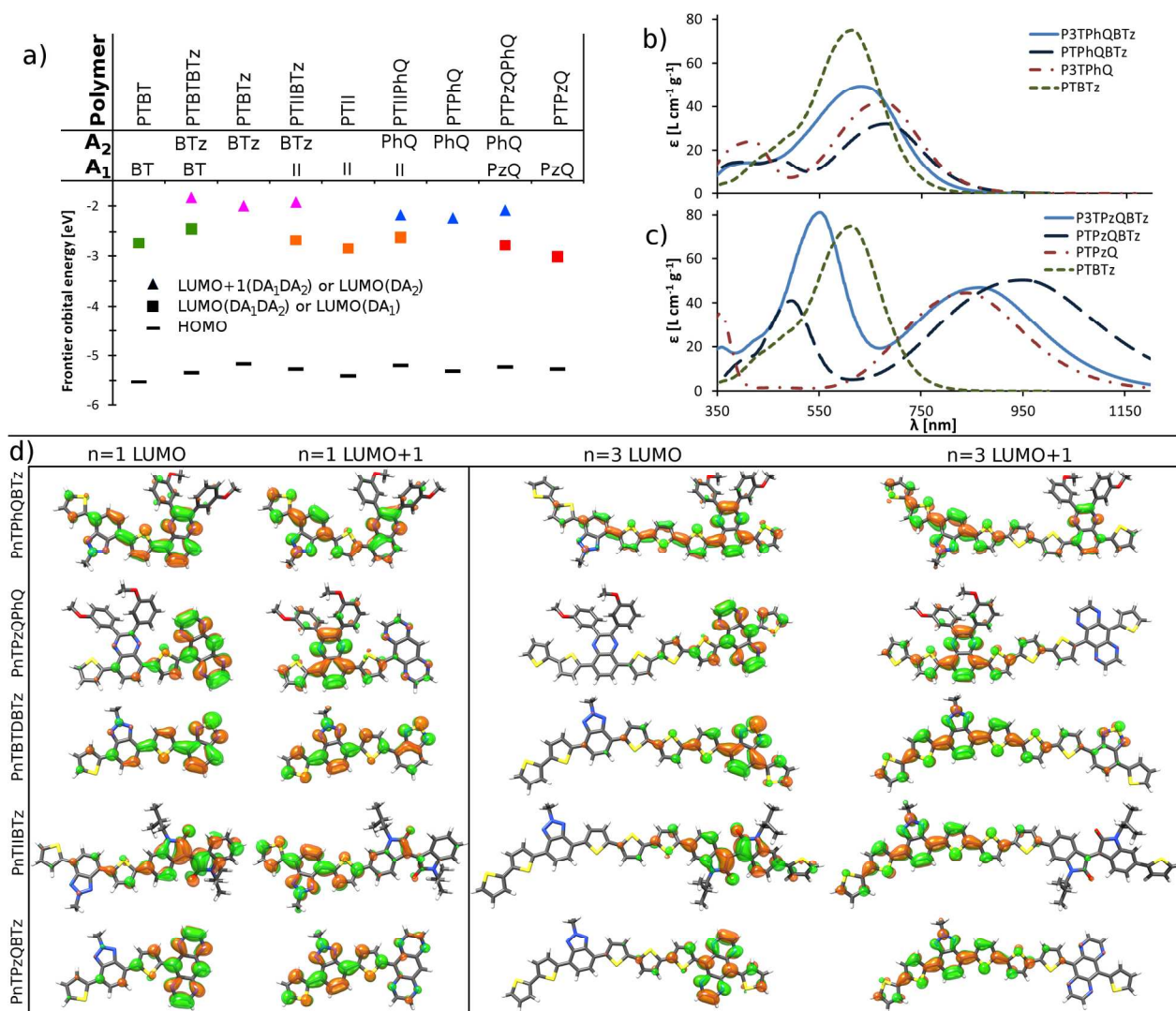LUMO(A_1)–LUMO(A_2) mixing afforded by a short donor and small $\Delta E_{LUMO,A}$.

Figure 5. Calculated frontier orbital energies of a few representative D–A$_1$–D–A$_2$ polymers (one repeating unit) compared to the corresponding D–A polymers with a T donor and A$_1$ or A$_2$ (two repeating units), demonstrating the agreement between the D–A LUMO to the corresponding D–A$_1$–D–A$_2$ LUMO or LUMO+1 (a). Calculated spectra of PnTPhQBTz (b) and PnTPzQBTz (c) compared to their corresponding D–A polymer calculated spectra. LUMO and LUMO+1 of the 10 computational D–A$_1$–D–A$_2$ polymers, sorted by increasing $\Delta E_{LUMO,A}$ (d). LUMO is densest on the stronger acceptor, and LUMO+1 on the weaker acceptor, but the localization is dependent on donor length and $\Delta E_{LUMO,A}$. Orbital isovalue=0.025.

The maximum absorption coefficients ε_{max} of the second absorption feature vary greatly, from 81

$\text{Lg}^{-1}\text{cm}^{-1}$ for P3TPzQBTz to 9 $\text{Lg}^{-1}\text{cm}^{-1}$ for PTPzQPhQ, appearing positively influenced by donor

length and also qualitatively correlating to $\Delta E_{LUMO,A}$, see spectra in Figure 4 and listed ε_{max} in

Table 4. This is rationalized from an analogy between the $D–A_1$ and $D–A_2$ parts and an excitonic

J-dimer. With sufficiently strong excited state interaction, the total excited state wave functions

$\Psi(S_1)$ and $\Psi(S_2)$, with corresponding transition dipole moments $M(S_1)$ and $M(S_2)$ are described

by Equation 4. C is a prefactor that is equal to $2^{-1/2}$ in the case of identical chromophores and ψ_1

and ψ_2 are the wave functions of the non-interacting excitonic parts with transition dipole

moments μ_1 and μ_2, respectively, where the asterisk * denotes an excited wave function.[93]

$$\Psi(S_1) = C(\psi_1^*\psi_2 + \psi_1\psi_2^*) \quad M(S_1) = C(\mu_1 + \mu_2) \tag{4}$$

$$\Psi(S_2) = C(\psi_1^*\psi_2 - \psi_1\psi_2^*) \quad M(S_2) = C(\mu_1 - \mu_2)$$

With increasing interaction between the $D–A_1$ and $D–A_2$ excitonic parts, the transition to S_1 is

strengthened and S_2 is weakened, since the transition dipoles μ_1 and μ_2 are approximately parallel

along the polymer backbone. If conversely the excitonic interaction is small, the $D–A_1$ and $D–A_2$

absorb more independently of each other, and the $D–A_1–D–A_2$ spectrum resembles a combination

of the corresponding D–A polymer spectra. This is visualized in Figure 5b and 5c where the

calculated spectra of PnTPhQBTz and PnTPzQBTz are compared to their corresponding D–A

polymers: PTPzQ, P3TPhQ, and PTBTz, showing a clear resemblance for P3TPzQBTz whose

excitonic interaction is minimal (large $R(A_1–A_2)$ and $\Delta E_{LUMO,A}$). These D–A polymers display

large calculated absorption coefficients since they are based on the same small side-group ratio of

33 wt% as the $D–A_1–D–A_2$ polymers. The remaining three $D–A_1–D–A_2$ spectra are compared to

their corresponding D–A polymers in Figure S3 in the ESI. The very small $\Delta E_{LUMO,A}$ in

PnTPzQPhQ and PnTPhQBTz result in such strong excitonic interaction and small calculated

second $\varepsilon_{max} \leq 28$ Lg^{-1}cm^{-1}, that this secondary absorption feature is likely to be indistinguishable

in experimental spectra, similar to the case for PTQTI in Figure 2a.

Table 4. Wavelengths (λ) and absorption coefficients (ε), of the 1st (peak) and 2nd (peak or

shoulder) calculated absorption features, as well as difference in LUMO energy between the two

acceptors ($\Delta E_{LUMO,A}$).

	PnTPhQBTz	**PnTPzQPhQ**	**PnTBTBTz**	**PnTIIBTz**	**PnTPzQBTz**
n=1 λ_1 [nm]	681	924	730	630	954
n=3 λ_1 [nm]	643	882	667	618	866
n=1 λ_2 [nm]	467	580	483	444	496
n=3 λ_2 [nm]	552	647	532	517	550
n=1 ε_1 [Lg^{-1}cm^{-1}]	32.4	35.6	63.6	64.6	50.9
n=3 ε_1 [Lg^{-1}cm^{-1}]	51.4	39.6	67.8	67.5	47.3
n=1 ε_2 [Lg^{-1}cm^{-1}]	15.9	9.1	36.1	41.2	41.1
n=3 ε_2 [Lg^{-1}cm^{-1}]	14.1	28.1	51.4	59.2	81.2
$\Delta E_{LUMO,A}$ [eV]	0.73	0.97	1.17	1.55	1.70

The light-harvesting capabilities of polymers in OPVs are reflected by the resulting device

external quantum efficiency (EQE) which depends on the active layer (polymer + fullerene)

absorbance A. The integration of the EQE with the solar emission spectrum gives the current of

the cell. The calculated solution mass absorption coefficients of the polymer ε(poly) and of the

fullerene $\varepsilon(PC_{71}BM)$ can be used for a rough estimation of the theoretical short circuit current J_{SC}, using a number of assumptions: film thickness d=100 nm, film densities ρ=1 g cm^{-3}, a 1:1 polymer:PC$_{71}$BM mass ratio, full reflectivity of the bottom electrode yielding two optical passes through the active layer, and an internal quantum efficiency IQE=100% for all polymers, *i.e.* absorbed photons produce one charge each. In addition, the transition dipole moments are assumed to be perfectly parallel to the backbones of the polymers, which during spin-coating become parallel to the surface of the film. This increases the polymer absorption by a factor 1.5 compared to an 3D-isotropic solution.[94–96] Using these assumptions, the calculated solution absorption coefficients ε are transformed to film EQE according to Equation 5, and integrated with the AM 1.5 solar spectral photon flux $\Phi_{e\lambda}$ [s^{-1} m^{-2} nm^{-1}], providing an approximate estimation of J_{SC}. This permits a valuable qualitative comparison of the light-harvesting potential between polymers, although the approximations are too rough for quantitative predictions, neglecting *e.g.* effects of optical interference, internal reflection, diffuse scattering, and crystallinity.[97]

$$J_{SC}^{theo} = q_e \int_0^\infty \Phi_{e\lambda}^{sol} \text{EQE} \, d\lambda \approx q_e \int_0^\infty \Phi_{e\lambda}^{sol}(1 - 10^{-A}) \, d\lambda$$

$$\approx q_e \sum_{\lambda=350}^{2000} \Phi_{e\lambda}^{sol} \left(1 - 10^{-\frac{2d\rho(1.5\varepsilon(poly)+\varepsilon(PC71BM))}{2}} \right) \qquad (5)$$

The theoretical J_{SC} as calculated for the thirteen D–A$_1$–D–A$_2$ polymers in this and the previous section are listed in Table 5.The polymers with 3T donors yield greater theoretical J_{SC}s than the T donor polymers for most acceptor combinations, since their secondary peaks/shoulders absorb more strongly and at longer λ where the solar emission is more intense. Only in PnTBTBTz does the appreciable 1st peak redshift with the shorter T donor lead to larger estimated currents than

the 3T case. Of the ten computationally modelled polymers, P3TPzQBTz exhibits the greatest

theoretical J_{SC}. However, the very strong PzQ acceptor usually causes unfavorably low

copolymer LUMO energies, hampering the driving force for electron transfer to the fullerene,

thus limiting the device IQE, J_{SC}, and fill factor (FF).[98–101] For the same reasons of having too

low LUMO energy, PBBTDPP is discarded for OPV applications. The PnTBTBTz, PnTIIBTz,

and PBTDPP polymers accordingly emerge as D–A$_1$–D–A$_2$ polymer candidates with excellent

spectral coverage and concomitant driving force for charge separation at the fullerene/polymer

interface.

Table 5. Theoretical J_{SC} of the D–A$_1$–D–A$_2$ polymer, obtained according to Equation 5. For the

sake of fair comparison, PTQTI, PBTDPP, and PBBTDPP were here assumed to have the same

side-chain ratio of 33 wt% as the 10 computationally modelled polymers.

Polymer	$J_{SC,theo}$ [mA/cm^2]	
	(n=1)	(n=3)
PnTPhQBTz	14.8	16.9
PnTPzQPhQ	21.2	27.3
PnTBTBTz	24.2	21.2
PnTIIBTz	18.2	18.3
PnTPzQBTz	27.9	30.4
PTQTI	15.4	
PBTDPP	28.0	
PBBTDPP	35.8	

Proof of concept –Two D–A₁–D–A₂ polymers with superior spectral coverage

Proceeding from the knowledge obtained from the systematic computational investigation in the previous section, two promising D–A₁–D–A₂ polymers P3TQTIF and PTIIBTzF were selected for further experimental and theoretical examination. Their structures are presented in Chart 3. They both employ isoindigo as the stronger acceptor, chosen for its good spectral and electronic properties, with LUMO energies suitably aligned to PCBM LUMO.[63,62,102–105] P3TQTIF was recently synthesized and exhibits a PCE of over 7%, attributed in part to its broad absorption.[33] PTIIBTzF is here synthesized for the first time. It is a fluorinated variation of one of the best light-harvesters from the previous section. Fluorination of BTz has previously been shown to improve the performance of D–A polymers with this acceptor,[56,73,74,106] due to a lowering of the HOMO/LUMO levels, but also to an increase in absorption strength.

Chart 3. Chemical structures of P3TQTIF and PTIIBTzF.[a]
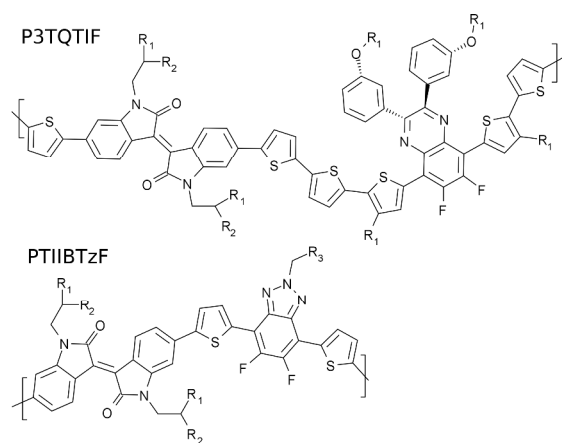
[a]R₁=1'-octyl, R₂=1'-hexyl, R₃=5'-undecyl.

The experimental solution spectra for the two D–A_1–D–A_2 polymers are compared to the

computationally predicted spectra in Figure 6a and 6b, as calculated with TD-DFT and applying

Equation 3. Similarly to Figure 2, the calculated predictions in Figure 6 show good agreement

with experiments concerning both relative and absolute peak intensities, as well as peak

wavelengths. For both polymers, the calculated predictions overestimate the ε_{max} and E_{abs}

slightly. While P3TQTIF displays only one resolved absorption feature $\geq$ 450 nm, the spectrum

of PTIIBTzF reveals a pronounced secondary peak at ~450 nm. PTIIBTzF exhibits a calculated

ε_{max} practically identical to the non-fluorinated PTIIBTz: 55 $Lg^{-1}cm^{-1}$ if using the experimental

side-chain mass, and 63 $Lg^{-1}cm^{-1}$ if assuming 33 wt% side-chains as in the previous section. The

calculated first peak λ_{max} blue-shifts by 19 nm upon fluorination, which is rationalized from the

placement of the fluorine atoms on the BTz acceptor where LUMO has negligible density,

leading to greater stabilization of HOMO than of LUMO. The second peak λ_{max} is redshifted with

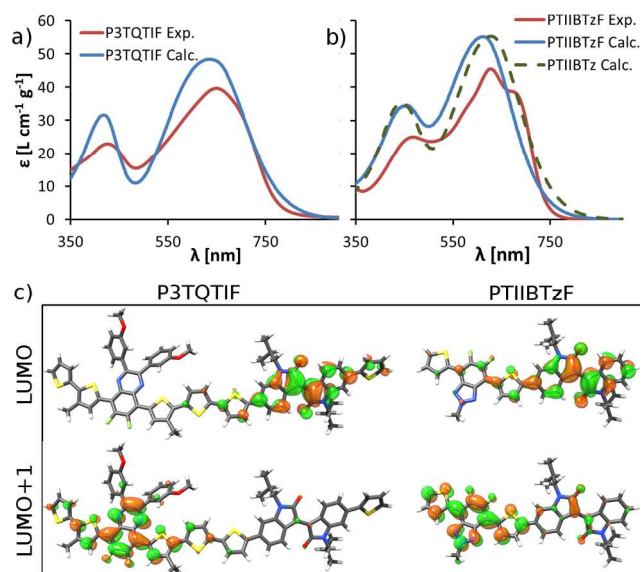fluorination due to a stabilization of LUMO+1.

Figure 6. Absorption spectra, experimental and as calculated, of P3TQTIF (a), and PTIIBTzF, compared its non-fluorinated variant PTIIBTz (b). Monomer LUMO and LUMO+1 of both P3TQTIF and PTIIBTzF, partly localized on the respective stronger and weaker acceptors (c). Orbital isovalue=0.025.

The electronic transitions for P3TQTIF and PTIIBTzF were calculated with TD-DFT for both mono- and dimers. The monomer results are presented in Table 6, due to the more pure orbital and transition characteristics of these smaller systems compared to dimers. Table 6 reveals a behavior analogous to that of the 10 polymers from the previous section: the two strongest low energy excitations are of respectively HOMO→LUMO and HOMO→LUMO+1 character. Copolymer LUMO and LUMO+1 again correspond mainly to the LUMOs of the respective acceptors, see Figure 6c. See Table S1 in the ESI for orbital energies, and Figure S4 in the ESI for the HOMO and LUMO+2 orbitals.

Table 6. Wavelengths, oscillator strengths, dominant orbital contributions, and the percentage of that contribution of the four strongest calculated transitions for P3TQTIF and PTIIBTzF monomers.[a]

	P3TQTIF				PTIIBTzF		
λ_{abs} [nm]	f	Orbitals	C [%]	λ_{abs} [nm]	f	Orbitals	C [%]
658	1.57	H→L	86.7	558	0.93	H→L	90.2
573	0.43	H→L+1	89.3	462	0.26	H-2→L	44.6
539	0.13	H-1→L	66.4	423	0.63	H→L+1	89.8
425	1.05	H→L+2	58.1	302	0.14	H→L+2	70.7

[a]H=HOMO, L=LUMO.

In PTIIBTzF the transitions to LUMO and LUMO+1 are responsible for the two respective absorption peaks, as demonstrated in Table 6 and Figure 6c. For P3TQTIF conversely, the absorption peak at ~400 nm in P3TQTIF is a non-CT, $\pi \rightarrow \pi^*$ transition, analogous to the typical case for D–A polymers. The HOMO→LUMO+1 transition in P3TQTIF is too weak and too close in wavelength to the stronger HOMO→LUMO transition for it to be resolved as a secondary peak or even a discernable shoulder. However, this CT transition to PhQ is the reason for the particularly wide absorption peak as seen here in Figure 6a and as previously reported for P3TQTIF, thus contributing to its total light-harvesting capability and the resulting excellent J_{SC} and good PCE of 15.5 mA/cm^2 and 7.0 %.[33] This demonstrates that the D–A$_1$–D–A$_2$ motif can be advantageous even when the two absorption features in the low-energy region are not resolved. The theoretical J_{SC}s based on calculated solution spectra, introduced in Equation 5, amount to 15.4 and 17.2 mA/cm^2 for P3TQTIF and PTIIBTzF respectively, assuming 33 wt% side-chains.

This rough estimate is for P3TQTIF highly similar to the experimental J_{SC}, which most probably involves some fortuitous cancellation of errors.

P3TQTIF exhibits better spectral coverage than most D–A polymers. But the fact that it is poorer than for many of the D–A$_1$–D–A$_2$ polymers studied here, and yet produces an impressive experimental J_{SC} of 15.5 mA/cm^2, is very encouraging for the continued development of new D–A$_1$–D–A$_2$ polymers. For example, BTz combined with BT or II acceptors constitute copolymer designs which here are predicted to display superior spectral coverage compared to existing polymers.

Conclusions

The D–A$_1$–D–A$_2$ motif for conjugated polymers is attractive for organic photovoltaic (OPV) purposes, already having achieved a 7% PCE in bulk heterojunction solar cells.[33] Their advantage over D–A polymers resides in their potential for enhanced spectral coverage facilitated by employing two acceptors with complementary absorption properties. However, the molecular electronic structure governing the optical properties of D–A$_1$–D–A$_2$ has not previously been studied in a systematic way. We here use a DFT-based computational strategy to assess the electronic and optical traits of 15 D–A$_1$–D–A$_2$ copolymer candidates, with careful comparison to selected experimental spectra warranting the validity of the calculations.

All polymers show intense primary absorption peaks originating from electronic transitions HOMO→LUMO, where LUMO mainly corresponds to the LUMO of the stronger acceptor. Copolymer LUMO+1 predominantly displays character of the weaker acceptor LUMO, and electronic transitions to this orbital are responsible for additional absorption features ~450–650

nm. The intensity and wavelength of these secondary features are shown to be strongly dependent on the respective acceptor LUMOs' separation in space ($R(A_1-A_2)$) and energy ($\Delta E_{LUMO,A}$). This is rationalized from a MO argument: the two acceptor LUMOs interact and mix, forming the copolymer LUMO and LUMO+1, where the degree of mixing is proportional to $e^{-R(A-A)}/\Delta E_{LUMO,A}$, affecting the λ_{max} splitting between the 1st and 2nd absorption peaks. The second peak/shoulder intensity is positively influenced by a small $LUMO(A_1)$–$LUMO(A_2)$ interaction, to the point where for weak interactions, the absorption profile of the $D-A_1-D-A_2$ polymer appears similar to a combination of the corresponding two D–A polymer spectra. For the strong LUMO–LUMO mixing cases conversely, the first transition dominates and the addition of the second acceptor loses its effect on the optical response of the polymer. Consequently, copolymers with the weak BTz acceptor and an adequately strong acceptor such as II or BT display excellent spectral coverage *via* dual peak absorption, and are expected to result in efficient OPVs, in particular if combined with a spatially separating donor segment such as terthiophene.

In a broader perspective, strictly alternating $D-A_1-D-A_2$ polymers are still uncommon, although the motif has proven its ability to yield efficient solar cells due to an enhanced spectral coverage with potential for additional absorption features $\gtrsim 450$ nm, where the solar emission is intense. These features derive from optically allowed charge-transfer transitions to the LUMO+1 of the copolymers, an excitation which normally is forbidden in D–A polymers. The $D-A_1-D-A_2$ concept thus constitutes a fundamentally advantageous fourth strategy to extend the spectral coverage of polymer solar cells, beyond tandem, ternary, or polymer–polymer solar cells. We demonstrate the usefulness of quantum chemical calculations, offering deeper insight into the structure–property relation with respect to the choice of acceptors and donor, and the resulting optical and electronic properties of copolymers. The accuracy of the calculations is furthermore

demonstrated to approach the level required for quantitative prediction of absorption spectra. Our computational approach serves to guide the development of new $D–A_1–D–A_2$ polymers with superior light-harvesting capabilities. Specifically, we advise the design of copolymers with three key parameters: 1) a similarly strong intrinsic absorptivity of $D–A_1$ and $D–A_2$, and a weak $LUMO(A_1)–LUMO(A_2)$ interaction as achieved by 2) extended donor segments and 3) substantial difference in LUMO energy between the two acceptors. The success of this approach for rational design of polymers with superior spectral coverage was, to conclude, demonstrated through the proof-of-concept synthesis and characterization of two new $D–A_1–D–A_2$ polymers with excellent light-harvesting capabilities.

Electronic supplementary information

Electronic supplementary information (ESI) available: $D–A_1–D–A_2$ planarity and calculated frontier orbital energies. List of electronic transitions as calculated with TD-PBE0, comparing gas phase to PCM calculations. Correlation between acceptor unit LUMO energies, copolymer LUMO energies, and second absorption peak/shoulder intensity. LUMO+2 for P3TQTIF and PTIIBTzF. Synthesis details for PTIIBTzF.

Disclosure statement

The authors declare no competing financial interest.

Acknowledgements

References

1 N. E. Jackson, B. M. Savoie, T. J. Marks, L. X. Chen and M. A. Ratner, *J. Phys. Chem. Lett.*, 2015, **6**, 77–84.

2 E. Wang, W. Mammo and M. R. Andersson, *Adv. Mater.*, 2014, **26**, 1801–1826.

3 Y. Li, *Acc. Chem. Res.*, 2012, **45**, 723–733.

4 G. Li, R. Zhu and Y. Yang, *Nat. Photonics*, 2012, **6**, 153–161.

5 H. Zhou, L. Yang and W. You, *Macromolecules*, 2012, **45**, 607–632.

6 Y. Liu, J. Zhao, Z. Li, C. Mu, W. Ma, H. Hu, K. Jiang, H. Lin, H. Ade and H. Yan, *Nat. Commun.*, 2014, **5**.

7 J. You, L. Dou, K. Yoshimura, T. Kato, K. Ohya, T. Moriarty, K. Emery, C.-C. Chen, J. Gao, G. Li and Y. Yang, *Nat. Commun.*, 2013, **4**, 1446.

8 J. Y. Kim, K. Lee, N. E. Coates, D. Moses, T.-Q. Nguyen, M. Dante and A. J. Heeger, *Science*, 2007, **317**, 222–225.

9 Z. Tang, Z. George, Z. Ma, J. Bergqvist, K. Tvingstedt, K. Vandewal, E. Wang, L. M. Andersson, M. R. Andersson, F. Zhang and O. Inganäs, *Adv. Energy Mater.*, 2012, **2**, 1467–1476.

10 W. Li, A. Furlan, K. H. Hendriks, M. M. Wienk and R. A. J. Janssen, *J. Am. Chem. Soc.*, 2013, **135**, 5529–5532.

11 E. Zhou, J. Cong, Q. Wei, K. Tajima, C. Yang and K. Hashimoto, *Angew. Chem. Int. Ed.*, 2011, **50**, 2799–2803.

12 W. Li, W. S. C. Roelofs, M. Turbiez, M. M. Wienk and R. A. J. Janssen, *Adv. Mater.*, 2014, **26**, 3304–3309.

13 Y. Zhou, T. Kurosawa, W. Ma, Y. Guo, L. Fang, K. Vandewal, Y. Diao, C. Wang, Q. Yan, J. Reinspach, J. Mei, A. L. Appleton, G. I. Koleilat, Y. Gao, S. C. B. Mannsfeld, A. Salleo, H. Ade, D. Zhao and Z. Bao, *Adv. Mater.*, 2014, **26**, 3767–3772.

14 P. P. Khlyabich, B. Burkhart and B. C. Thompson, *J. Am. Chem. Soc.*, 2012, **134**, 9074–9077.

15 L. Lu, T. Xu, W. Chen, E. S. Landry and L. Yu, *Nat. Photonics*, 2014, **8**, 716–722.

16 Y. Gu, C. Wang, F. Liu, J. Chen, O. E. Dyck, G. Duscher and T. P. Russell, *Energy Environ. Sci.*, 2014, **7**, 3782–3790.

17 F. Goubard and G. Wantz, *Polym. Int.*, 2014, **63**, 1362–1367.

18 T. Ameri, P. Khoram, J. Min and C. J. Brabec, *Adv. Mater.*, 2013, **25**, 4245–4266.

19 A. Facchetti, *Mater. Today*, 2013, **16**, 123–132.

20 C. R. McNeill, *Energy Environ. Sci.*, 2012, **5**, 5653–5667.

21 B. Burkhart, P. P. Khlyabich and B. C. Thompson, *ACS Macro Lett.*, 2012, **1**, 660–666.

22 V. Tamilavan, K. H. Roh, R. Agneeswari, D. Y. Lee, S. Cho, Y. Jin, S. H. Park and M. H. Hyun, *J. Mater. Chem. A*, 2014, **2**, 20126–20132.

23 J.-M. Jiang, H.-C. Chen, H.-K. Lin, C.-M. Yu, S.-C. Lan, C.-M. Liu and K.-H. Wei, *Polym. Chem.*, 2013, **4**, 5321–5328.

24 J. W. Jung, F. Liu, T. P. Russell and W. H. Jo, *Energy Environ. Sci.*, 2013, **6**, 3301–3307.

25 D. Dang, W. Chen, R. Yang, W. Zhu, W. Mammo and E. Wang, *Chem. Commun.*, 2013, **49**, 9335–9337.

26 W. Sun, Z. Ma, D. Dang, W. Zhu, M. R. Andersson, F. Zhang and E. Wang, *J. Mater. Chem. A*, 2013, **1**, 11141–11144.

27 A. J. Kronemeijer, E. Gili, M. Shahid, J. Rivnay, A. Salleo, M. Heeney and H. Sirringhaus, *Adv. Mater.*, 2012, **24**, 1558–1565.

28 P. Sonar, S. P. Singh, Y. Li, M. S. Soh and A. Dodabalapur, *Adv. Mater.*, 2010, **22**, 5409–5413.

29 S. Albert-Seifried, D.-H. Ko, S. Huttner, C. Kanimozhi, S. Patil and R. H. Friend, *Phys. Chem. Chem. Phys.*, 2014, **16**, 6743–6752.

30 J. D. Yuen, J. Fan, J. Seifter, B. Lim, R. Hufschmid, A. J. Heeger and F. Wudl, *J. Am. Chem. Soc.*, 2011, **133**, 20799–20807.

31 S. Subramaniyan, F. S. Kim, G. Ren, H. Li and S. A. Jenekhe, *Macromolecules*, 2012, **45**, 9029–9037.

32 B. Balan, C. Vijayakumar, A. Saeki, Y. Koizumi and S. Seki, *Macromolecules*, 2012, **45**, 2709–2719.

33 Q. Tao, Y. Xia, X. Xu, S. Hedström, O. Bäcke, D. I. James, P. Persson, E. Olsson, O. Inganäs, L. Hou, W. Zhu and E. Wang, *Macromolecules*, 2015, **48**, 1009–1016.

34 T. E. Kang, K.-H. Kim and B. J. Kim, *J. Mater. Chem. A*, 2014, **2**, 15252–15267.

35 A. Rauk, *Orbital Interaction Theory of Organic Chemistry*, Wiley, New York, 2004.

36 S. Hedström, P. Henriksson, E. Wang, M. R. Andersson and P. Persson, *Phys. Chem. Chem. Phys.*, 2014, **16**, 24853–24865.

37 S. Hedström and P. Persson, *J. Phys. Chem. C*, 2012, **116**, 26700–26706.

38 N. E. Jackson, B. M. Savoie, K. L. Kohlstedt, T. J. Marks, L. X. Chen and M. A. Ratner, *Macromolecules*, 2014, **47**, 987–992.

39 S. Mothy, M. Guillaume, J. Idé, F. Castet, L. Ducasse, J. Cornil and D. Beljonne, *J. Phys. Chem. Lett.*, 2012, **3**, 2374–2378.

40 H. Ma, T. Qin and A. Troisi, *J. Chem. Theory Comput.*, 2014, **10**, 1272–1282.

41 M. Frisch, G. Trucks, H. Schlegel, G. Scuseria, M. Robb, J. Cheeseman, G. Scalmani, V. Barone, B. Mennucci, G. Petersson, H. Nakatsuji, M. Caricato, X. Li, H. Hratchian, A. Izmaylov, J. Bloino, G. Zheng, J. Sonnenberg, M. Hada, M. Ehara, K. Toyota, R. Fukuda, J. Hasegawa, M. Ishida, T. Nakajima, Y. Honda, O. Kitao, H. Nakai, T. Vreven, J. Montgomery, J. Peralta, F. Ogliaro, M. Bearpark, J. Heyd, E. Brothers, K. Kudin, V. Staroverov, R. Kobayashi, J. Normand, K. Raghavachari, A. Rendell, J. Burant, S. Iyengar, J. Tomasi, M. Cossi, N. Rega, J. Millam, M. Klene, J. Knox, J. Cross, V. Bakken, C. Adamo, J. Jaramillo, R. Gomperts, R. Stratmann, O. Yazyev, A. Austin, R. Cammi, C. Pomelli, J. Ochterski, R. Martin, K. Morokuma, V. Zakrzewski, G. Voth, P. Salvador, J. Dannenberg, S. Dapprich, A. Daniels, Farkas, J. Foresman, J. Ortiz, J. Cioslowski and D. Fox, 2009.

42 W. Kohn and L. J. Sham, *Phys. Rev.*, 1965, **140**, A1133.

43 C. Adamo and V. Barone, *J. Chem. Phys.*, 1999, **110**, 6158–6170.

44 R. Ditchfield, W. J. Hehre and J. A. Pople, *J. Chem. Phys.*, 1971, **54**, 724–728.

45 E. Runge and E. K. U. Gross, *Phys. Rev. Lett.*, 1984, **52**, 997–1000.

46 R. Bauernschmitt and R. Ahlrichs, *Chem. Phys. Lett.*, 1996, **256**, 454–464.

47 M. Petersilka, U. J. Gossmann and E. K. U. Gross, *Phys. Rev. Lett.*, 1996, **76**, 1212–1215.

48 M. E. Casida, C. Jamorski, K. C. Casida and D. R. Salahub, *J. Chem. Phys.*, 1998, **108**, 4439–4449.

49 P. Atkins and R. Friedman, *Molecular Quantum Mechanics*, Oxford University Press, New York, 4th edn., 2005.

50 J. Cornil, I. Gueli, A. Dkhissi, J. C. Sancho-García, E. Hennebicq, J. P. Calbert, V. Lemaur, D. Beljonne and J. L. Brédas, *J. Chem. Phys.*, 2003, **118**, 6615–6623.

51 W. K. Ford, C. B. Duke and W. R. Salaneck, *J. Chem. Phys.*, 1982, **77**, 5030–5039.

52 T. T. Steckler, X. Zhang, J. Hwang, R. Honeyager, S. Ohira, X.-H. Zhang, A. Grant, S. Ellinger, S. A. Odom, D. Sweat, D. B. Tanner, A. G. Rinzler, S. Barlow, J.-L. Brédas, B. Kippelen, S. R. Marder and J. R. Reynolds, *J. Am. Chem. Soc.*, 2009, **131**, 2824–2826.

53 J. Tao, S. Tretiak and J.-X. Zhu, *Phys. Rev. B*, 2009, **80**, 235110.

54 B. Hu and J. Zhang, *Polymer*, 2009, **50**, 6172–6185.

55 S. Hedström, P. Henriksson, E. Wang, M. R. Andersson and P. Persson, *J. Phys. Chem. C*, 2015, **119**, 6453–6463.

56 S. C. Price, A. C. Stuart, L. Yang, H. Zhou and W. You, *J. Am. Chem. Soc.*, 2011, **133**, 4625–4631.

57 Y. Zhang, S.-C. Chien, K.-S. Chen, H.-L. Yip, Y. Sun, J. A. Davies, F.-C. Chen and A. K.-Y. Jen, *Chem. Commun.*, 2011, **47**, 11026–11028.

58 H. J. Son, W. Wang, T. Xu, Y. Liang, Y. Wu, G. Li and L. Yu, *J. Am. Chem. Soc.*, 2011, **133**, 1885–1894.

59 J. D. Yuen, R. Kumar, D. Zakhidov, J. Seifter, B. Lim, A. J. Heeger and F. Wudl, *Adv. Mater.*, 2011, **23**, 3780–3785.

60 T. L. Dexter Tam, T. Salim, H. Li, F. Zhou, S. G. Mhaisalkar, H. Su, Y. M. Lam and A. C. Grimsdale, *J. Mater. Chem.*, 2012, **22**, 18528–18534.

61 G. L. Schulz, M. Mastalerz, C.-Q. Ma, M. Wienk, R. Janssen and P. Bäuerle, *Macromolecules*, 2013, **46**, 2141–2151.

62 R. Stalder, J. Mei and J. R. Reynolds, *Macromolecules*, 2010, **43**, 8348–8352.

63 E. Wang, Z. Ma, Z. Zhang, K. Vandewal, P. Henriksson, O. Inganäs, F. Zhang and M. R. Andersson, *J. Am. Chem. Soc.*, 2011, **133**, 14244–14247.

64 T. Lei, Y. Cao, X. Zhou, Y. Peng, J. Bian and J. Pei, *Chem. Mater.*, 2012, **24**, 1762–1770.

65 H. Zhou, L. Yang, S. Xiao, S. Liu and W. You, *Macromolecules*, 2010, **43**, 811–820.

66 P. M. Beaujuge, C. M. Amb and J. R. Reynolds, *Acc. Chem. Res.*, 2010, **43**, 1396–1407.

67 G. L. Gibson, T. M. McCormick and D. S. Seferos, *J. Am. Chem. Soc.*, 2011, **134**, 539–547.

68 W. K. Chan, Y. Chen, Z. Peng and L. Yu, *J. Am. Chem. Soc.*, 1993, **115**, 11735–11743.

69 K. H. Hendriks, G. H. L. Heintges, V. S. Gevaerts, M. M. Wienk and R. A. J. Janssen, *Angew. Chem. Int. Ed.*, 2013, **52**, 8341–8344.

70 Y. Lee, Y. M. Nam and W. H. Jo, *J. Mater. Chem.*, 2011, **21**, 8583–8590.

71 D. Dang, W. Chen, S. Himmelberger, Q. Tao, A. Lundin, R. Yang, W. Zhu, A. Salleo, C. Müller and E. Wang, *Adv. Energy Mater.*, 2014, **4**, 1400680.

72 X. Xu, Z. Li, O. Backe, K. Bini, D. I. James, E. Olsson, M. R. Andersson and E. Wang, *J. Mater. Chem. A*, 2014, **2**, 18988–18997.

73 J. Min, Z.-G. Zhang, S. Zhang and Y. Li, *Chem. Mater.*, 2012, **24**, 3247–3254.

74 J. Min, Z.-G. Zhang, M. Zhang and Y. Li, *Polym. Chem.*, 2013, **4**, 1467–1473.

75 R. L. Uy, L. Yan, W. Li and W. You, *Macromolecules*, 2014, **47**, 2289–2295.

76 A. Tanimoto and T. Yamamoto, *Macromolecules*, 2006, **39**, 3546–3552.

77 N. Akbaşoğlu, A. Balan, D. Baran, A. Cirpan and L. Toppare, *J. Polym. Sci. Polym. Chem.*, 2010, **48**, 5603–5610.

78 K. H. Hendriks, G. H. L. Heintges, M. M. Wienk and R. A. J. Janssen, *J. Mater. Chem. A*, 2014, **2**, 17899–17905.

79 J. Torras, J. Casanovas and C. Alemán, *J. Phys. Chem. A*, 2012, **116**, 7571–7583.

80 G. R. Hutchison, Y.-J. Zhao, B. Delley, A. J. Freeman, M. A. Ratner and T. J. Marks, *Phys. Rev. B*, 2003, **68**, 035204.

81 J. Gierschner, J. Cornil and H.-J. Egelhaaf, *Adv. Mater.*, 2007, **19**, 173–191.

82 A. J. Cohen, P. Mori-Sánchez and W. Yang, *Science*, 2008, **321**, 792–794.

83 E. S. Kadantsev, M. J. Stott and A. Rubio, *J. Chem. Phys.*, 2006, **124**, 134901.

84 U. Salzner, P. G. Pickup, R. A. Poirier and J. B. Lagowski, *J. Phys. Chem. A*, 1998, **102**, 2572–2578.

85 Y. Zhao and D. G. Truhlar, *J. Phys. Chem. A*, 2006, **110**, 13126–13130.

86 A. Dreuw, J. L. Weisman and M. Head-Gordon, *J. Chem. Phys.*, 2003, **119**, 2943–2946.

87 T. Körzdörfer, J. S. Sears, C. Sutton and J.-L. Brédas, *J. Chem. Phys.*, 2011, **135**, 204107.

88 T. Tsuneda and K. Hirao, *Wiley Interdiscip. Rev. Comput. Mol. Sci.*, 2014, **4**, 375–390.

89 L. Pandey, C. Doiron, J. S. Sears and J.-L. Bredas, *Phys. Chem. Chem. Phys.*, 2012, **14**, 14243–14248.

90 P. Salvatori, E. Mosconi, E. Wang, M. Andersson, M. Muccini and F. De Angelis, *J. Phys. Chem. C*, 2013, **117**, 17940–17954.

91 Z. Ma, E. Wang, M. E. Jarvid, P. Henriksson, O. Inganäs, F. Zhang and M. R. Andersson, *J. Mater. Chem.*, 2012, **22**, 2306–2314.

92 B. C. Schroeder, Z. Huang, R. S. Ashraf, J. Smith, P. D'Angelo, S. E. Watkins, T. D. Anthopoulos, J. R. Durrant and I. McCulloch, *Adv. Funct. Mater.*, 2012, **22**, 1663–1670.

93 G. Lanzani, *The Photophysics behind Photovoltaics and Photonics*, Wiley, New York, 2012.

94 M. Campoy-Quiles, M. I. Alonso, D. D. C. Bradley and L. J. Richter, *Adv. Funct. Mater.*, 2014, **24**, 2116–2134.

95 M. Campoy-Quiles, P. G. Etchegoin and D. D. C. Bradley, *Phys. Rev. B*, 2005, **72**, 045209.

96 G. M. Marshall, G. P. Lopinski, F. Bensebaa and J. J. Dubowski, *Langmuir*, 2009, **25**, 13561–13568.

97 G. F. Burkhard, E. T. Hoke and M. D. McGehee, *Adv. Mater.*, 2010, **22**, 3293–3297.

98 Q. Peng, X. Liu, Y. Qin, J. Xu, M. Li and L. Dai, *J. Mater. Chem.*, 2011, **21**, 7714–7722.

99 F. Zhang, J. Bijleveld, E. Perzon, K. Tvingstedt, S. Barrau, O. Inganäs and M. R. Andersson, *J. Mater. Chem.*, 2008, **18**, 5468–5474.

100   Yi Zhou, D. A. Gedefaw, S. Hellström, I. Krätschmer, F. Zhang, W. Mammo, O. Inganäs and M. R. Andersson, *IEEE J. Sel. Top. Quantum Electron.*, 2010, **16**, 1565–1572.

101   S. Hellström, F. Zhang, O. Inganäs and M. R. Andersson, *Dalton Trans.*, 2009, 10032–10039.

102   L. Fang, Y. Zhou, Y.-X. Yao, Y. Diao, W.-Y. Lee, A. L. Appleton, R. Allen, J. Reinspach, S. C. B. Mannsfeld and Z. Bao, *Chem. Mater.*, 2013, **25**, 4874–4880.

103   Z. Ma, W. Sun, S. Himmelberger, K. Vandewal, Z. Tang, J. Bergqvist, A. Salleo, J. W. Andreasen, O. Inganäs, M. R. Andersson, C. Muller, F. Zhang and E. Wang, *Energy Environ. Sci.*, 2014, **7**, 361–369.

104   Y. Deng, J. Liu, J. Wang, L. Liu, W. Li, H. Tian, X. Zhang, Z. Xie, Y. Geng and F. Wang, *Adv. Mater.*, 2014, **26**, 471–476.

105   R. Stalder, J. Mei, K. R. Graham, L. A. Estrada and J. R. Reynolds, *Chem. Mater.*, 2013, **26**, 664–678.

106   F. M. Pasker, M. F. G. Klein, M. Sanyal, E. Barrena, U. Lemmer, A. Colsmann and S. Höger, *J. Polym. Sci. Polym. Chem.*, 2011, **49**, 5001–5011.